

MOX-Report No. 06/2020

**Image-based displacements analysis and computational  
blood dynamics after endovascular aneurysm repair**

Domanin, M.; Piazzoli, G.; Trimarchi, S.; Vergara, C.

MOX, Dipartimento di Matematica  
Politecnico di Milano, Via Bonardi 9 - 20133 Milano (Italy)

[mox-dmat@polimi.it](mailto:mox-dmat@polimi.it)

<http://mox.polimi.it>

# **IMAGE-BASED DISPLACEMENTS ANALYSIS AND COMPUTATIONAL BLOOD DYNAMICS AFTER ENDOVASCULAR ANEURYSM REPAIR**

Maurizio Domanin <sup>1-2</sup>, Giulia Piazzoli <sup>3</sup>, Santi Trimarchi <sup>1-2</sup>, Christian Vergara <sup>4</sup>

1 Department of Clinical Sciences and Community Health, Università di Milano, Italy

2 Unità Operativa di Chirurgia Vascolare, Fondazione I.R.C.C.S. Cà Granda Ospedale Maggiore Policlinico di Milano, Italy

3 MOX, Dipartimento di Matematica, Politecnico di Milano

4 LABS, Dipartimento di Chimica, Materiali e Ingegneria Chimica, Politecnico di Milano

Maurizio Domanin MD [maurizio.domanin@unimi.it](mailto:maurizio.domanin@unimi.it) <https://orcid.org/0000-0001-7510-3520>

Giulia Piazzoli PhD [giulia.piazzoli@polimi.it](mailto:giulia.piazzoli@polimi.it) <https://orcid.org/0000-0003-2694-1979>

Santi Trimarchi MD, PhD [santi.trimarchi@unimi.it](mailto:santi.trimarchi@unimi.it) <https://orcid.org/0000-0001-5996-3264>

Christian Vergara Eng [christian.vergara@polimi.it](mailto:christian.vergara@polimi.it) <https://orcid.org/0000-0001-9872-5410>

## **Abstract**

### **Purpose.**

To examine intra heartbeat displacements (IHD) and geometrical changes over years, defined as follow-up displacements (FUD), of the endograft for abdominal aortic aneurysm repair, and to correlate them with computational fluid dynamics (CFD). Despite the widespread diffusion of endovascular aneurysm repair (EVAR) we still do not know very much about endograft behavior after deployment.

### **Methods.**

Two cases, treated with expanded polytetrafluoroethylene (PTFE) on nitinol stent frame (PI) and with woven polyester fabric sutured to stainless steel Z-stent skeleton (PII), respectively, were submitted to dynamic computed tomography angiography (CTA) at 1, 12 and 60 months. After segmentation, IHD were computed as displacements of the reconstructed surface with respect to the diastolic instant.

Similarly, FUD were studied using imaging techniques that align temporal successive segmentations. At last, numerical simulations for blood dynamics were performed to compute viscous forces i.e. Wall Shear Stress (WSS) and Time Average WSS (TAWSS).

**Results.** IHD analysis showed slight translations without deformation for PI endograft with respect to the stiffer stainless steel endograft behaviour of PII. FUD showed in PI motion of the metallic struts mainly focused in the distal main body and in overlapping zone with iliac branches while in PII we observed a huge FUD in the middle and inferior-anterior regions of the main body. CFD analysis revealed changes of velocity patterns associated to remodelling of the iliac zone for PI and of the main body region for PII, where flow impinges the lumen wall and progressively provokes deformation of the endograft wires. TAWSS exhibits flow disturbances in the enlarged region coherently with displacements analysis.

**Conclusion.** Image-based displacements analysis associated to CFD allow to perform very subtle evaluations of endograft behaviour on different temporal scales. This kind of study could be helpful both for physicians, forecasting evolution during the life span of the endograft, and for manufacturers, giving them useful indication about endograft implant and design.

**Keywords** abdominal aortic aneurysm, endograft, stent-graft, dynamics computed tomography angiography, computational fluid dynamics

## **Introduction**

Endovascular aortic repair (EVAR) consists of inserting an endograft within the abdominal aortic aneurysm (AAA) to exclude the sac from the bloodstream and thereby eliminate the risk of growth and rupture. Almost all the available endografts are composed by a metal stent covered with fabric, bifurcated and modular to expand treatment options to different lengths and shape of AAAs. Currently, EVAR has gained so much diffusion among the surgical community to become the preferred treatment. This choice is closely associated to its lower invasiveness with respect to the conventional open surgical repair. Other advantages consist in less blood loss, shorter procedure times, lower rates of major adverse events and quicker recovery.

In patients with large AAAs, treatment by EVAR reduced the 30-day operative mortality by two-thirds with respect to open surgery [1]. Anyway, lifelong postprocedural surveillance is necessary after EVAR to assess for complications. Complications rates could be as high as 30% with a need for late interventions of 15-18% with an annual rate of 3.7%/year [2-4]. One of the most important of such complications is *graft migration*, that is defined as movement greater than 5 mm of the stent-graft from its initial deployment site [5-6].

Blood pulsatile drag forces play an important role in determining the movement of the stent graft [7-8]. Accordingly, the endograft deeply changes the mechanical behaviour of the aortic wall, the geometries of the vascular lumen and the hemodynamics with respect to the native AAA.

Analysis of medical imaging over follow-ups of the same patients, has revealed in the last 20 years a powerful tool to evaluate the graft migration [9]. In Zarins et al [10], the authors determined the distance of the endograft from the renal arteries to the proximal end of the stent after 5 years, whereas Benharash et al [11] measured on preoperative, post-implantation, and 1-year CTA scans the longitudinal centerline distance from the superior mesenteric artery. For more recent studies that quantified the stent movement by means of follow-up images, see [12-14].

Other studies have performed a Computational Fluid Dynamics (CFD) analysis to find possible correlations with stent graft migration. A first group of works focused on the study of the influence of blood dynamics through geometric factors on the forces exerted on the graft, [15-16] for the influence of the neck angle in ideal and real geometries, respectively, [7] for the influence of aortic curvature, [17] for the influence of the aortic flow, [18] for the case of fenestrated stents, [19] for the effect on the graft fixation, and [8,20-21] for the influence of endoleaks. Other works studied the different blood dynamics before and after the insertion of the graft [22-24], whereas a validation against experimental measures was performed in [24]. Instead, Figueroa et al [7] correlated blood dynamics with the graft migration obtained by follow-up imaging.

The aim of the present study was twofold. First, we have computed the endograft intra heartbeat displacements (IHD) due to the heart pulsation by means of dynamics 4D computed tomography angiography (CTA) imaging. These results were then put in relation with blood dynamics obtained by CFD in the same geometries.

Secondly, following [7], we have computed the displacement on the endograft over different interval of time, e.g. after one and five years, owing to CTA images at interval follow-up (follow-up displacements, FUD). Again, such displacements have been analysed together with the corresponding CFD in order to find possible qualitative correlations.

These findings allowed us to understand some important underlying processes that occurred with time on endograft behaviour, e.g. movements and efforts on the skeleton of the endograft and development of potential complications such as fatigue of metallic struts, migration or disconnection between different components (e.g. the main aortic body and iliac branches). Thus, possibly, this could give useful indication about endograft implant and design.

## **Material and Methods**

### *Ethics statement.*

The study has been approved by the Ethics Committee according to institutional ethics guidelines. All the patients gave their signed consent for the publication of data.

### *Clinical data*

Two patients (PI and PII in what follows) were submitted to EVAR due to high risks condition, hostile abdomen or patient preference. Aneurysms were classified as small ( $< 5$  mm), medium (5.0 to 6.5 mm) or large ( $> 6.5$  mm), according to the recommendations of the Society for Vascular Surgery/International Society for Cardiovascular Surgery reporting subcommittee [25]. Both patients were treated by EVAR as elective surgery. PI had an history of poliomyelitis who affected the right leg. He was a heavy smoker and was submitted three years before to bilateral embolectomy during a travel in Eastern Asia for acute limb ischemia secondary to iliac-femoral thrombosis. During the perioperative assessment a very small AAA (3 cm  $<$ ) was detected. Since then, he was yearly submitted to Doppler Ultrasound (DUS) follow up. Last DUS revealed sudden growth of the AAA's diameter up to 4.4 cm in absence of inner thrombus and its shape was saccular and asymmetrical. PII had a medical history of previous sigmoid resection for colorectal neoplasia eight years before the diagnosis of AAA. EVAR was preferred because of the condition of hostile abdomen. PII has a more common fusiform-shaped AAA with an inner laminar thrombus inside the sac.

In both the cases, after five years of clinical and CTA follow up, we have not reported post-operative complications. Moreover, over the years we observed the complete shrinking of the AAA's sac for PI and its reduction (20%) for PII (Tab. 1).

The endograft used for PI is composed by a nitinol stent frame attached to expanded polytetrafluoroethylene (PTFE) and covered with a thin, non-permeable layer of fluorinated ethylene propylene. The main body has a single docking limb used in

combination with different iliac limbs. Usually, it is bimodular but in this case it was used in a tri-fab way, since the patient was tall and a more distal iliac landing was needed. Instead, the endograft used for PII has a modular bifurcated design composed by the main aortic body with an assortment of iliac limbs. The fabric is made of woven polyester graft material, hand sutured to the stainless steel Z-stent graft skeleton. This endograft is available in a standard three-part design. In both the cases, the bifurcation is proximally respect to the aneurysm sac [26].

### *Image processing*

For each case, 4-dimensional CT with Siemens SOMATOM Definition AS scanner (Siemens Medical Solutions, Erlangen, Germany) have been acquired. Non-ionic contrast media (Iomeron, Bracco, Milan, Italy) was used with a concentration of 400 mg/ml, 1.5 cc pro kg, and an injection speed of 3 cc/s. The total effective dose resulted 34 mSv for each case. Ten ECG gated series of axial images were then reconstructed at every 10% of the R-R interval from the aortic arch to the common femoral arteries. This approach allows the retrieval of dynamic imaging of the aorta and stent graft during a complete systolic-diastolic cycle.

We have obtained imaging for two patients under study. For each of them we have different acquisitions obtained at 1 months (T1), 12 months (T12) and 60 months (T60).

In particular for PI:

PI-T1: reconstruction matrix: 512 x 512 x 926, slice thickness 1.5 mm;

PI-T12: reconstruction matrix: 512 x 512 x 715, slice thickness 1.5 mm;

PI-T60: reconstruction matrix: 512 x 512 x 717, slice thickness 1.5 mm;

and PII:

PII-T1: reconstruction matrix: 512 x 512 x 1002, slice thickness 0.6 mm;

PII-T12: reconstruction matrix: 512 x 512 x 1001, slice thickness 1.5 mm;

PII-T60: reconstruction matrix: 512 x 512 x 607, slice thickness 1.5 mm.

Since stent-grafts are characterized by sharp corners of the wire, small wire diameter, leaks and gaps due to artifacts which blood vessels do not feature, methods developed for vascular elements segmentation are not suitable for stent graft wires reconstruction.

For this reason, a manual segmentation with a level-set algorithm implemented in VMTK ([www.vmtk.org](http://www.vmtk.org)) has been performed. This was possible since the wires of the stent-grafts are highly visible in CT scans being made of nitinol, a radiopaque material.

In order to eliminate all structures that are not strictly the stent-graft, such as vertebral bones, a procedure that isolates the circular structures separating them from other structures and connects them together has been in some cases used (Fig. 1a).

Once we had at disposal the geometric surfaces of the endograft of each patient for each frame of the heartbeat and for each follow up exam, we were ready to compute displacements.

To compute IHD, we evaluated the displacements of each point of the reconstructed surface with respect to the diastolic instant, i.e. the diastolic (7<sup>th</sup>) time frame among the available ten ones. Accordingly, we computed the point-wise minimum distance between two surfaces, considering from each point of the current surface the closest triangle on the reference surface. The distance was positive if the distance vector and the normal to the reference surface had negative dot product, i.e. if the current surface was for that specific point outer with respect to the reference surface.

Regarding the computation of FUD, we first needed to register the corresponding images. In particular, we considered the diastolic frame for each follow up image. To this aim, we used the Iterative Closest Point [27]. For each patient, the registrations were performed with respect to the coordinate system of the most recent follow-up. A rigid translation of the other follow up geometries was performed such that the renal arteries were aligned with those in the most recent follow up (Fig. 1b). Once registration was performed, we quantified FUD among follow-ups with a procedure similar to that used for IHD.

In view of the CFD analysis, surface models of the diastolic boundary lumen were reconstructed by using ITK-Snap (<http://www.itksnap.org>), which allowed us to better manage the high intensity of stent-graft in CT images. Such models were then converted into volumetric meshes composed by tetrahedral with three layers of boundary layers. We performed a refinement study with respect to space discretization, by testing that the results on WSS remained the same, up to a tolerance of 2%, when

reducing the mesh size of a factor 20%. Accordingly, we have considered a characteristic mesh size equal to about 0.15 cm for all the cases (Fig. 1c).

### *Computational fluid-dynamics*

We considered unsteady numerical simulations for blood dynamics performed by using the Finite Elements library LifeV (<http://www.lifev.org>). Blood was assumed Newtonian and incompressible, and due to the presence of the stent the assumption of rigid walls was made. Unlike the pre-operative case, where the sudden change of geometric shape induced by the aneurysm lead to transition to turbulence [28-29], we consider here a laminar flow. These assumptions are well accepted for our cases since the diameter of the vessels is greater than 0.6 cm and flow rate is quite moderate [30]. The blood density was set equal to 1.06 g/cm<sup>3</sup>, whereas the viscosity to 0.035 Poise. As for the boundary conditions, at the inlet section, a representative physiological flow rate with a systolic peak of 120cm<sup>3</sup>/s [31] has been prescribed through the parabolic velocity profile assumption. Stress-free conditions were prescribed at the two outflow sections, that is the iliac districts, with a stabilization technique to overcome instabilities due to backflows [32].

We used a backward Euler scheme for time discretization, a linearization of the convective term, and P1-P1 Finite Elements stabilized by means of the SUPG-PSPG technique [33].

CPU time of simulations was about 15 hours for 2 heartbeats, where only the second one is considered for the analysis of the results.

As postprocessed blood dynamics quantity of interest, we considered Wall Shear Stress (WSS) that is the viscous forces exerted by blood on the endograft wall. In particular, we computed the mean WSS over the heartbeat, that is the Time Average WSS (TAWSS). This quantity is known to be correlated to formation of vortices in regions of low values [34] and it is proposed here to correlate blood dynamics with endograft displacements in region of elevated values.

## Results

### *Endograft intra heartbeat displacements (IHD)*

In Fig. 2a we report the endograft IHD of PI and PII between the systolic and diastolic instants. According to the definition given previously, red means outer displacements with respect to the reference, blue means inward displacements, whereas green means null normal displacements. For PI, we have found that maximum IHD was 0.81 mm for PI-T1, 0.90 mm for PI-T12 and 0.92 mm for PI-T60. Thus, from these results we concluded that PI was subjected to a rigid translation of the endograft, without any significant deformation. Regarding PII, from IHD computed for PII-T1, we observe an almost complete absence of any displacement, which suggested that PII endograft was

particularly motionless during the heartbeat. These findings were observed also for PII-T12 and PII-T60, not reported here.

#### *Endograft displacement over follow up (FUD)*

Regarding endograft FUD taken between diastolic frames in different follow-up CTA, we have reported three colour maps obtained from CTA imaging, that depict the FUD between T1 vs T12 (T1-T12), T12 vs T60 (T12-T60) and between T1 vs T60 (T1-T60) (Fig. 2b). From these results, we have observed a motion of the metallic struts of the endograft skeleton.

Major FUD in PI resulted mainly focused in proximity of the distal landing zones at the left iliac limb in T1-T12 and just after the bifurcation at the right iliac in T12-T60. With time, FUDs were localized also in the distal main body, in the zone of overlapping between the main body and the contralateral iliac branch and in the distal landing zone of the third iliac component. Regarding PII, we have observed a huge FUD in the middle and inferior-anterior regions of the main body and a moderate displacement at the origin of the right iliac region. The main displacement is associated to an enlargement of the main body graft struts along the flow direction. Major FUD started since the first year and maintained consistently this orientation with time.

To quantify these FUD, we have reported the maximum displacements for all the cases at the level of the aortic main body and at the iliac branches (Tab. 2). From these results, we have observed significant FUD of the endograft in the order of some (even up to 8)

millimeters for all the cases reported. As expected, in accordance with Fig. 2b, we can notice also that FUD increases with time.

### *Qualitative correlations with blood dynamics*

To assess the evolution of blood dynamics over time, we report in Fig. 3 as an illustrative example the velocity field at several cross sections for PI-T1 and PI-T60. From these results, we observe that the velocity patterns change significantly with time. Moreover, we observe that a region of the right iliac tract (section D) changed its dimensions as a consequence of an enlargement (Fig. 3).

In all the three follow-up computational domains of PI, we have then computed the systolic WSS by CFD analyses and we have matched them with IHD (Fig. 4a). From these results, we notice for PI-T1 and PI-T12 a rigid behaviour of the left iliac branch in correspondence of the region with highest WSS values (see regions highlighted with arrows in Fig. 4a). On the contralateral side, i.e. the right iliac branch where hypoplasia of the arteries and a supplemental overlap between two endograft components were present due to the specific choice of tri-fab configuration, we have noticed focal elevated WSS both in PI-T1 and PI-T12 with consequent rigid displacements. Moreover, in PI-T60 we have observed a reduction of both the values and the extension area of WSS according to the remodelling of the right iliac zone.

Regarding PII, we found that the systolic WSS values are smaller than in the previous case (less than one half) and this could justify the fact the no significant IHD were noticed for this patient.

In the second analysis, we have tried to find correlations between blood dynamics and FUD. To this aim, we have analysed CFD results obtained for PI in T1 putting them in relation with T1-T12 FUD, and then the CFD results obtained in T12 have been put in relation with T12-T60 FUD. The idea was to see if specific blood dynamics patterns at a given follow-up could be an indicator to predict displacement of the graft at the next follow-up.

We have reported TAWSS and FUD over two consecutive follow-up data (Fig. 4b). We have observed for PI elevated values of TAWSS at the right hypoplastic region which seem to be correlated with the largest FUD values mainly observed in T12-T60 (see arrows in Fig. 4b). Regarding PII, who underwent to a significant eccentric deformation in the aortic region over the years, we have plotted TAWSS and systolic velocity field together with FUD in the same plot (Fig. 5). In particular, we have considered three cases: CFD in T1 together with T1-T12 FUD; CFD in T12 together with T1-T12 FUD; CFD in T60 together with T12-T60 FUD. From these results, we have observed that blood, which initially flows in caudal and slightly anterior direction, impinges the lumen wall at the aortic bending point. The reduction in velocity causes the flow to become unstable, leading to flow separation and recirculation. The expansion of the stent-graft wires results located exactly where such flow disturbances takes place. Accordingly, we have observed that TAWSS exhibits lower values in the enlarged region with respect to adjacent areas, coherently with the disturbed flow computation.

## **Discussion**

EVAR treatment has revolutionized the treatment of AAAs. The rationale of EVAR is the depressurization of sac deploying the endograft, distal to renal arteries, in a proximal neck of at least 1.5 cm, without significant calcification or thrombus, and similarly distal in the iliac arteries with a landing zone of at least 2.0 cm.

The endograft is usually composed by two or three overlapped segments deployed in short landing zone. Moreover, it is subjected to millions of heartbeats during the patient life. This continuous hemodynamic solicitation induces mechanical stress in the endograft that could be responsible of some of the late complications such as proximal neck enlargement, graft migration, endoleaks, fabric tear, stent fractures and graft thrombosis.

Fortunately, complications occur just only in a smaller percentage. Nevertheless, it is important to understand the behaviour of the endograft over long period of time, and also successful interventions could be helpful to achieve this aim.

Some aspects, such as drag forces and their role in endograft migration, are well known. Figueroa et al, observed three dimensional changes over time on post EVAR follow up CTA. Endografts showed displacement in all three spatial dimensions with prevalence on transverse and axial directions with orientation of displacement force mainly perpendicular to the greatest curvature of the endograft. Most of these endograft had migrations which required secondary treatment. [7]

Together with the most debated issue of drag forces, many other aspects of endografts behaviour, such as stiffness and structural changes in both the short and long term are still less explored.

Endograft deployment deeply modifies the mechanical behaviour of the AAA, since implantation of a rigid graft in the proximal neck might stiffen that aortic segment. [35] In this direction, our original results about IHD highlighted that the endograft behaves as a stiff body during the heartbeat. Looking further into the matter, constituent materials (nitinol vs stainless steel) and different design (exoskeleton covered with PTFE vs hand sutured dacron fabric to the stent structure) seem to lead to slightly different mechanical behaviours. Indeed, as expected, IHD analysis showed that in PI the endograft has a relatively more compliant behaviour with respect to PII that looks stiffer and less prone to adsorb aortic flow impingement (Fig. 2a). In any case, our analysis suggests that the deformability of these endografts during the heartbeat is less than the optimal/physiological one, as already observed in some reports [35-36].

Moreover, looking further, the IHD analysis highlighted regions, for example the area of overlap between the main aortic body and the left iliac branch for both PI and PII, where anisotropic displacements of the endograft were detected. For PI, this anisotropic behaviour is still relevant after 1 year but it seems to vanish after 5 years, according to the well-known stiffening of EVAR over years. It is known that anisotropic displacement of aortic aneurysms before the insertion of the graft may have an impact in growth and rupture [31, 37-39]. Thus, anisotropic displacements also in

presence of EVAR found here may have a clinical role that should be investigated in future studies.

On the other side, a significant permanent deformation over the years has been observed by our FUD results for both endografts. This phenomenon has been scarcely highlighted in cases without complications. In particular, endograft implanted in PII revealed almost twice the deformation with respect to PI. This could be again related to the specific design and material that characterized the endograft.

Moreover, we stress that the evolution of the endograft leads to a new hemodynamic configuration due to the formation of a synergic coupling AAA-endograft. [7] In recent years, CFD in bifurcated aortic endograft has been used by some authors to find correlations with stent graft migration evaluated by means of follow-up images [7-8, 15-24] and with the geometrical characterization of the EVAR-induced reshaping. [40] Here, we performed for the first time an attempt to find qualitative correlations between CFD and IHD. What we observed is that peak WSS for PI is higher in the regions of not negligible IHD and that it remarkably decreases for PI-T60 where the displacement is almost null (Fig. 4a). Accordingly, lower values of WSS are obtained for PII which experienced lower IHD.

Regarding follow-up analysis, CFD for PI showed that TAWSS is remarkable in regions of maximum FUD, i.e. at the overlap between the main aortic body and the iliac branches (Fig. 4b). Interestingly, with time the gently push outward of the nitinol together with the action of blood flow could have also led in this area to a remodelling of the right iliac region (section D in Fig. 3) accordingly to the reduction of WSS.

For PII, the more pronounced FUD of the main aortic body induced an enlargement of the metallic struts with significant blood vortex which increases with time (Fig. 5). In particular, the maximum deformations of the endograft resulted localized in the posterior region at T12. Moreover, at T60 we have noticed structural deformations mainly localized in the anterior region of the stainless steel skeleton. The maximum enlargement of the main aortic body section localized just over the bifurcation area is associated to the development of recirculation phenomena as confirmed by the low WSS values calculated at this site (Fig. 5). This specific behaviour of the stainless steel Z-stent graft has been also reported in Lin et al who compared in vitro twist fatigue in different devices. In particular, they observed that endografts with angled Z-shaped stents had a lower durability compared to ringer stent grafts. The major issue was a mechanical damage to the polyester fabric where the apices of adjacent stents form a sharp angle. [41]

Limitations of the present study are related to the small sample that is justified considering the exceptional nature of the imaging, not usually performed for clinical follow up, and the deal of work needed for the analysis of imaging and CFD computation.

Finally, we point out that for the CFD simulations, a rigid wall hypothesis was adopted, instead of performing a fluid-structure interaction analysis. This assumption was acceptable for our aims considering also the observed high stiffness of the aneurysmatic aortic portion treated by stent graft deployment.

## **Conclusions**

Currently EVAR has deeply changed the management of AAA and, when feasible, it represents the preferred treatment for most of the vascular specialists. Despite its widespread diffusion, we still do not know very much about endograft behavior after its deployment inside the AAA. The endografts are subjected to a huge and chronic mechanical stress exerted by the blood flow during the systolic-diastolic cycle. Hemodynamics generates modifications of the geometries and stress of the component materials of the endograft responsible for complications development that can occur earlier or later. Even in successful cases, the analysis of the endograft behaviour on different temporal scales by means of advanced imaging coupled with CFD, could be helpful for surgeons to analyze modification of the endograft during its life span forecasting the risk of complication development such as fatigue of the materials or disconnections between components. The modifications of the endograft structure after 60 months justifies the need for long-term, and possibly life-long surveillance after EVAR.

Moreover, the study of IHB and FUD can be useful also for endograft manufacturers to furtherly improve endograft conception, project and design. Currently, despite the great progress made in stent graft production, obtained thanks to the reduction of profiles and the improvement of fixation to the aortic wall, we are still far from to have ideal endografts with more physiological behavior and without long term durability concerns.

## REFERENCES

1. The UK EVAR Trial Investigators. Endovascular versus open repair of abdominal aortic aneurysm. *N Engl J Med.* 2010;362:1863-1871
2. Chang RW, Goodney P, Tucker LY et al. Ten-year results of endovascular abdominal aortic aneurysm repair from a large multicenter registry. *J Vasc Surg.* 2013;58:324–332.
3. Mehta M, Sternbach Y, Taggart JB et al. Long-term outcomes of secondary procedures after endovascular aneurysm repair. *J Vasc Surg.* 2010;52:1442–1448.
4. Nordon IM, Karthikesalingam A, Hinchliffe RJ et al. Secondary interventions following Endovascular Aneurysm Repair (EVAR) and the enduring value of graft surveillance. *Eur J Vasc Endovasc Surg.* 2010;39:547–554.
5. Resch T, Malina M, Lindblad B et al. The impact of stent graft design on proximal stent–graft fixation in the abdominal aorta: an experimental study. *Eur J Vasc Endovasc Surg.* 2000;20:190–195.
6. Chuter TAM. Stent–graft design: the good, the bad and the ugly. *Cardiovasc Surg.* 2002;10:7–13.
7. Figueroa CA, Taylor CA, Yeh V. Preliminary 3D computational analysis of the relationship between aortic displacement force and direction of endograft movement. *J Vasc Surg.* 2010;51:1488–1497.
8. Nolz R, Schwartz E, Langs G et al. Stent graft surface movement after infrarenal abdominal aortic aneurysm repair: comparison of patients with and without a type 2 endoleak. *Eur J Vasc Endovasc Surg.* 2015;50:181-188.
9. Resch T, Ivancev K, Brunkwall J et al. Distal migration of stent-grafts after endovascular repair of abdominal aortic aneurysms, *J Vasc Interv Rad.* 1999;10: 257-264.
10. Zarins CK, Bloch DA, Crabtree T et al. Stent graft migration after endovascular aneurysm repair: importance of proximal fixation. *J Vasc Surg.* 2003;38:1264-1272

11. Benharash P, Lee JT, Abilez OJ et al. Iliac fixation inhibits migration of both suprarenal and infrarenal aortic endografts. *J Vasc Surg.* 2007;45:250-7.
12. Kobayashi M, Hoshina K, Yamamoto S et al. Development of an image-based modeling system to investigate evolutional geometric changes of a stent graft in an abdominal aortic aneurysm. *Circ J.* 2015;79:1534-1541.
13. Nemoto Y, Hoshina K, Kobayashi M et al. Morphological changes and device migration after stent graft insertion - Clinical application of an image-based modeling system and analysis with geometric parameters. *Circ J.* 2017; 25;82:176-182.
14. López-Linares K, García I et al. Image-based 3D Characterization of abdominal aortic aneurysm deformation after endovascular aneurysm repair. *Front Bioeng Biotechnol.* 2019;7:267.
15. Morris L, Delassus P, Walsh M et al. A mathematical model to predict the *in vivo* pulsatile drag forces acting on bifurcated stent grafts used in endovascular treatment of abdominal aortic aneurysms (AAA). *J Biomech.* 2004;37:1087-1095.
16. Molony DS, Kavanagh EG, Madhavan P et al. A computational study of the magnitude and direction of migration forces in patient-specific abdominal aortic aneurysm stent-grafts. *Eur J Vasc Endovasc Surg.* 2010;40:332-339.
17. Stefanov F, McGloughlin T, Delassus P et al. Hemodynamic variations due to spiral blood flow through four patient-specific bifurcated stent graft configurations for the treatment of abdominal aortic aneurysms. *Int J Numer Method Biomed Eng.* 2013;29:179-196.
18. Sun Z, Chaichana T. Fenestrated stent graft repair of abdominal aortic aneurysm: hemodynamic analysis of the effect of fenestrated stents on the renal arteries. *Korean J Radiol.* 2010;11:95–106.
19. Morris L, Stefanov F, McGloughlin T. Stent graft performance in the treatment of abdominal aortic aneurysms: The influence of compliance and geometry. *J Biomech* 2013;46:383–395.
20. Wolters BJBM, Rutten MCM, Schurink GWH et al. Computational modelling of endoleak after endovascular repair of abdominal aortic aneurysms. *Int J Numer Meth Biomed Engng.* 2010;26:322–335.

21. Lu YH, Mani K, Panigrahi B et al. Endoleak assessment using computational fluid dynamics and image processing methods in stented abdominal aortic aneurysm models. *Comput Math Methods Med.* 2016;956:72-94.
22. Frauenfelder T, Lotfey M, Boehm T et al. Computational fluid dynamics: hemodynamic changes in abdominal aortic aneurysm after stent-graft implantation. *Cardiovasc Intervent Radiol.* 2006;29:613-623.
23. Molony DS, Callanan A, Kavanagh EG et al. Fluid-structure interaction of a patient-specific abdominal aortic aneurysm treated with an endovascular stent-graft. *BioMedical Engineering On Line.* 2009;8:24.
24. Raptis A, Xenos M, Georgakarakos E et al. Comparison of physiological and post-endovascular aneurysm repair infrarenal blood flow. *Comput Methods Biomech Biomed Engin.* 2017;20:242-249.
25. Ahn SS, Rutherford RB, Johnston KW et al. Reporting standards for infrarenal endovascular abdominal aortic aneurysm repair. Ad hoc committee for standardized reporting practises in vascular surgery of the Society of The Vascular Surgery/International Society for Cardiovascular Surgery. *J Vasc Surg.* 1997;25:405–410.
26. Eckroth-Bernard K, Garvin R et al. Current Status of Endovascular Devices to Treat Abdominal Aortic Aneurysms. *Biomed Eng Comput Biol.* 2013;5:25–32.
27. Besl P, McKay HD. A method for registration of 3-D shapes. *IEEE Trans Pattern Anal Mach Intell, Proceedings Volume 1611, Sensor Fusion IV: Control Paradigms and Data Structures,* 239–256, 1992.
28. Khanafer K, Bull J, Jr GU et al. Turbulence significantly increases pressure and fluid shear stress in an aortic aneurysm model under resting and exercise flow conditions. *Ann Vasc Surg.* 2007;21:67–74
29. Vergara C, Le Van D, Quadrio M et al. Large eddy simulations of blood dynamics in abdominal aortic aneurysms. *Med Eng Phys.* 2017;47:38-46.

30. Quarteroni A, Manzoni A, Vergara C. The Cardiovascular System: Mathematical Modeling, Numerical Algorithms, Clinical Applications. *Acta Numerica*. 2017;26:365-590.
31. Piccinelli M, Vergara C, Antiga L et al. Impact of hemodynamics on lumen boundary displacements in abdominal aortic aneurysms by means of dynamic computed tomography and computational fluid dynamics. *Biom Model Mech*. 2013;12:1263-1276.
32. Moghadam ME, Bazilevs Y, Hsia TY et al. A comparison of outlet boundary treatments for prevention of backflow divergence with relevance to blood flow simulations. *Computat Mech*. 2011;48:277–291.
33. Tezduyar TE, Stabilized Finite Element Formulations for Incompressible Flow Computations, *Adv Appl Mech*. 1991;28:1–44.
34. Ku DN, Giddens DP, Zarins CK et al. Pulsatile flow and atherosclerosis in the human carotid bifurcation. Positive correlation between plaque location and low oscillating shear stress. *Arteriosclerosis* 1985;5:293-302.
35. Morris L, Stefanov F, Hynes N et al. An experimental evaluation of device/arterial wall compliance mismatch for four stent graft devices and a multilayer flow modulator device for the treatment of abdominal aortic aneurysms. *Eur J Vasc Endovasc Surg*. 2016;51:44–55
36. Van Keulen JW, Prehn, Prokop M et al. Dynamics of the aorta before and after endovascular aneurysm repair: a systematic review. *Eur J Vasc Endovasc Surg*. 2009;38:586-596.
37. Vos AWF, Wisselink W, Marcus JT et al. Cine MRI assessment of aortic aneurysm dynamics before and after endovascular repair. *J Endovasc Ther*. 2003;10:433–439
38. Van Herwaarden JA, Bartels LW, Muhs BE et al. Dynamic magnetic resonance angiography of the aneurysm neck: conformational changes during the cardiac cycle with possible consequences for endograft and future design. *J Vasc Surg*. 2006;44:22–28
39. Arko FR, Murphy EH, Davis CM III et al. Dynamic geometry and wall thickness of the aortic neck of abdominal aortic aneurysms with intravascular ultrasonography. *J Vasc Surg*. 2007;46:891–897.

40. Tasso P, Raptis A, Matsagkas M, Lodi Rizzini M, Gallo D, Xenos M, Morbiducci U. Abdominal aortic aneurysm endovascular repair: profiling postimplantation morphometry and hemodynamics with image-based computational fluid dynamics. *J Biomech Eng.* 2018;140:111003.
41. Lin, J, Guidoin, R, Du, J An in vitro twist fatigue test of fabric stent-grafts supported by Z-Stents vs. ringed stents. *Materials* 2016; 9:113–113.

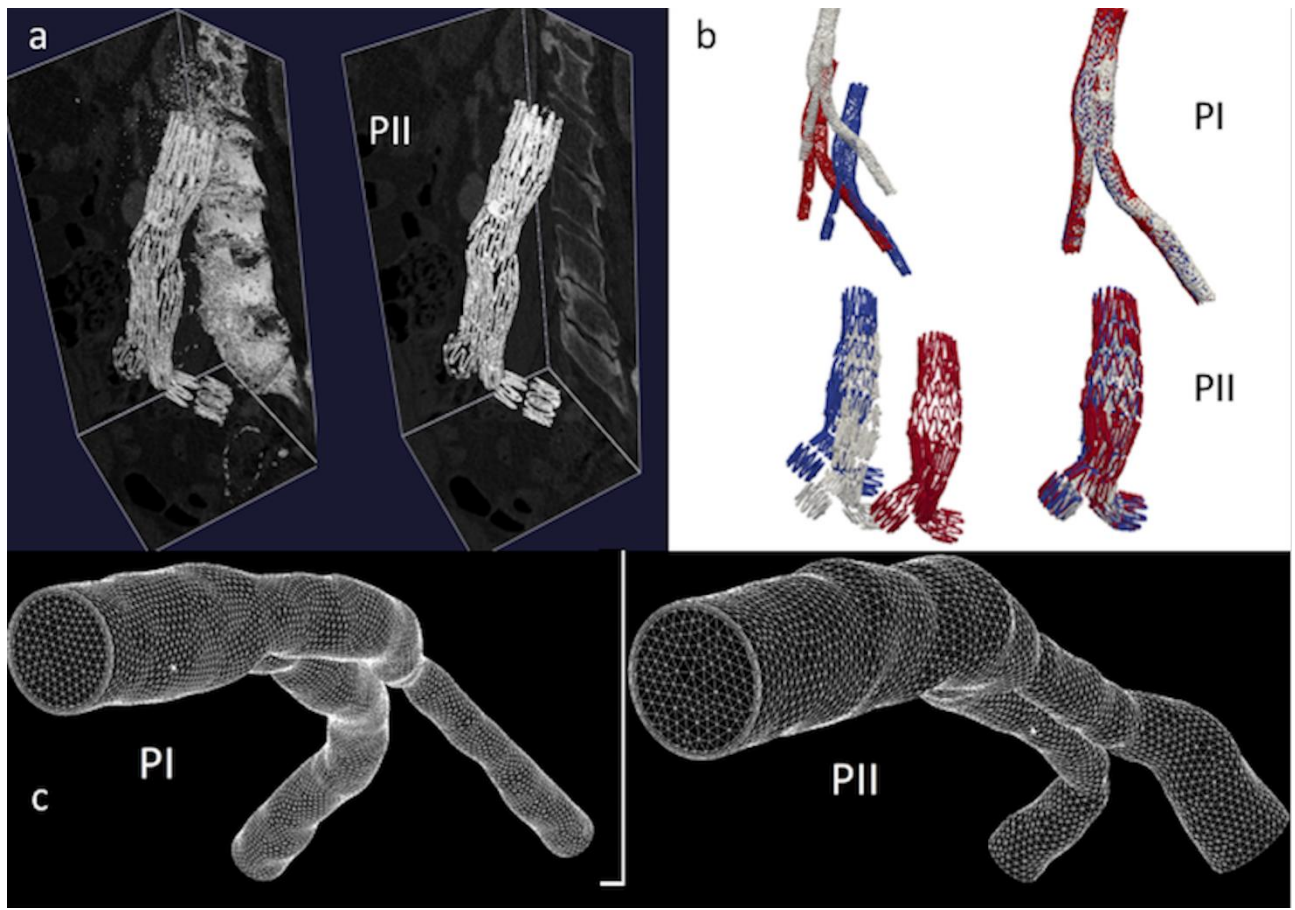


Fig. 1. a) PII: Example of stent reconstruction. Left: presence of artefacts and vertebral bones. Right: reconstruction after isolation procedure; b) PI (up) and PII (down): For each subpart on the left the segmentations T1 (white), T12 (blue) and T60 (red) with different coordinate systems. On the right the result of the registration; c) computational meshes for PI (left) and PII (right) in T1.

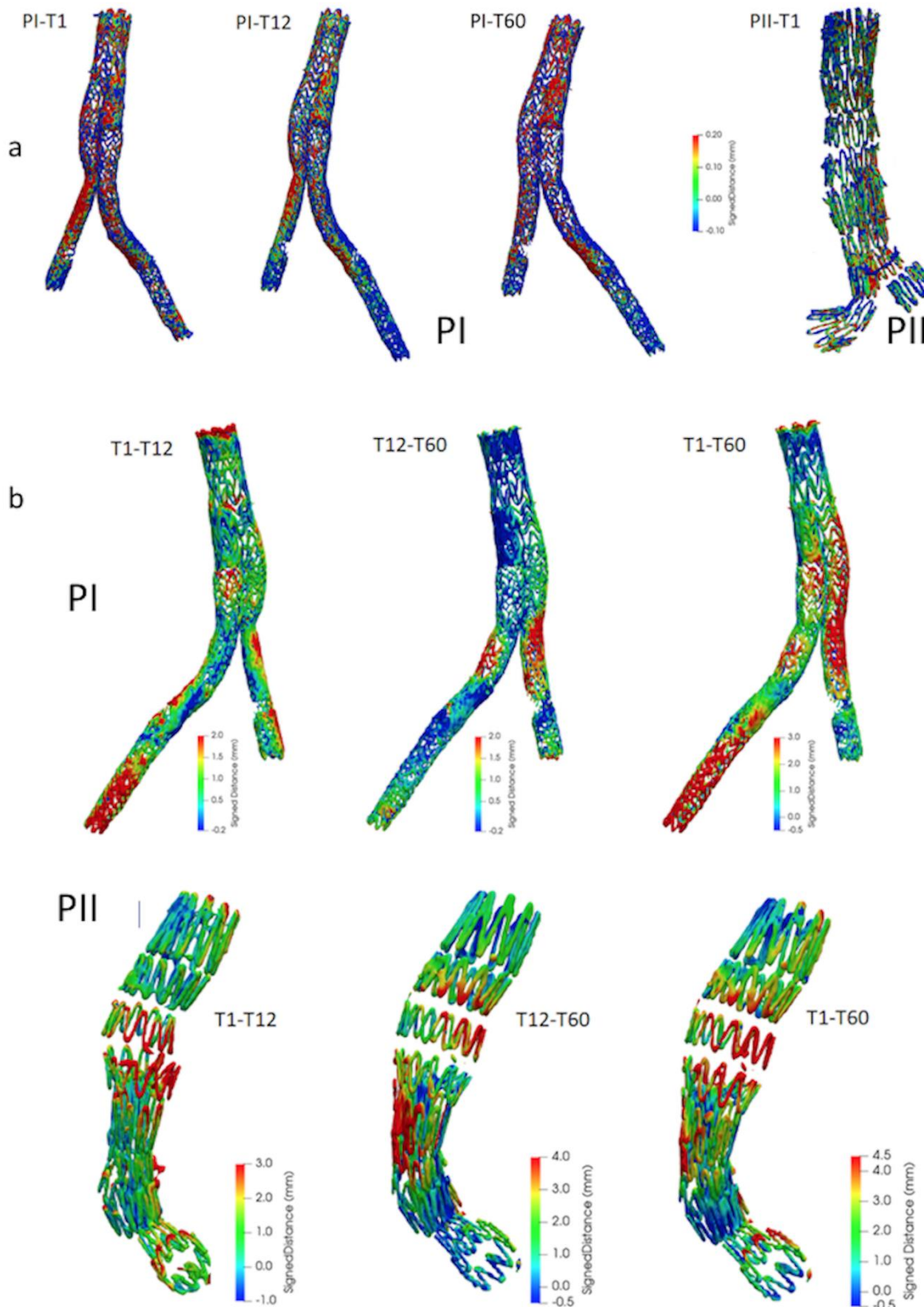


Fig. 2. a) Intra heartbeat displacements (IHD) of the graft between the third (systole) and the seventh (diastole) frames along the heartbeat in antero-posterior view for PI and posterior-anterior view for PII. Red means outer displacements with respect to the reference, blue means inward displacements whereas green means no displacements; b) Displacement over different interval of time (FUD). Red means outer displacements with respect to the reference, blue means inward displacements. PI: postero-anterior views; PII: left views.

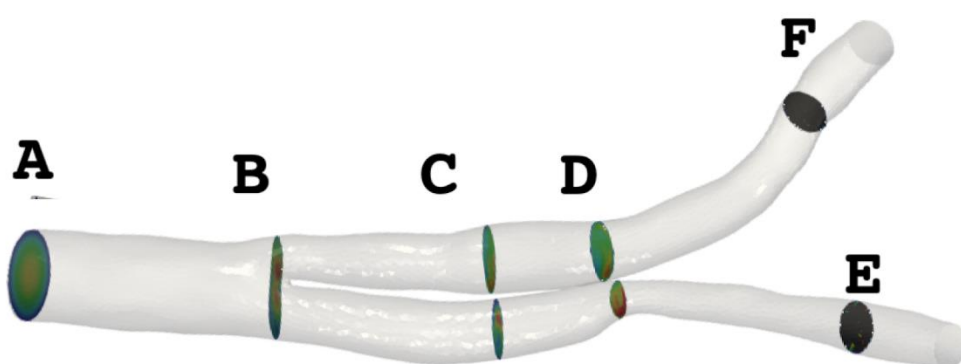
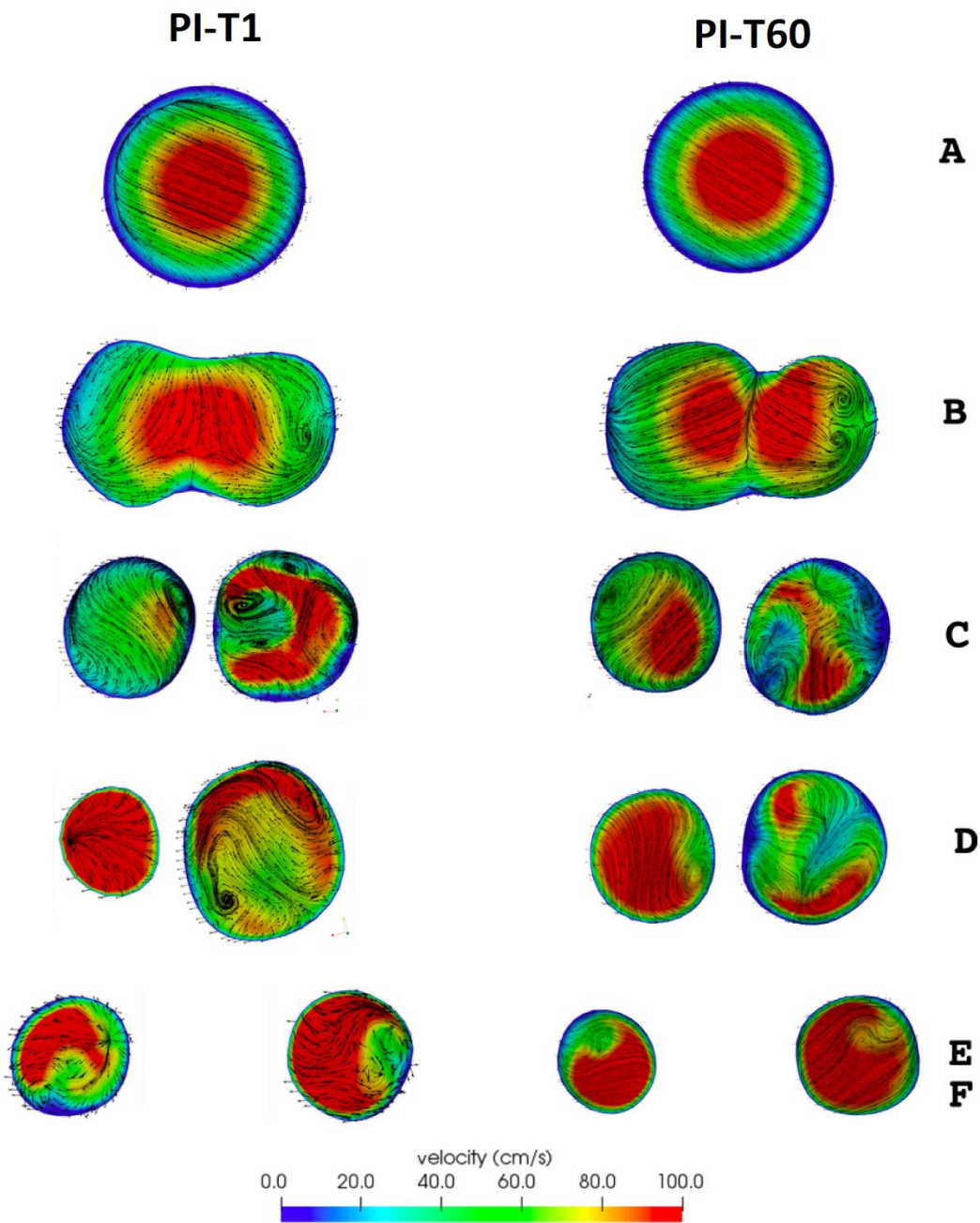


Fig. 3. Examples of the velocity field at several cross sections for PI-T1 and PI-T60. Velocity patterns change significantly with time. In particular, we observe remodelling in the right iliac segment (section D).

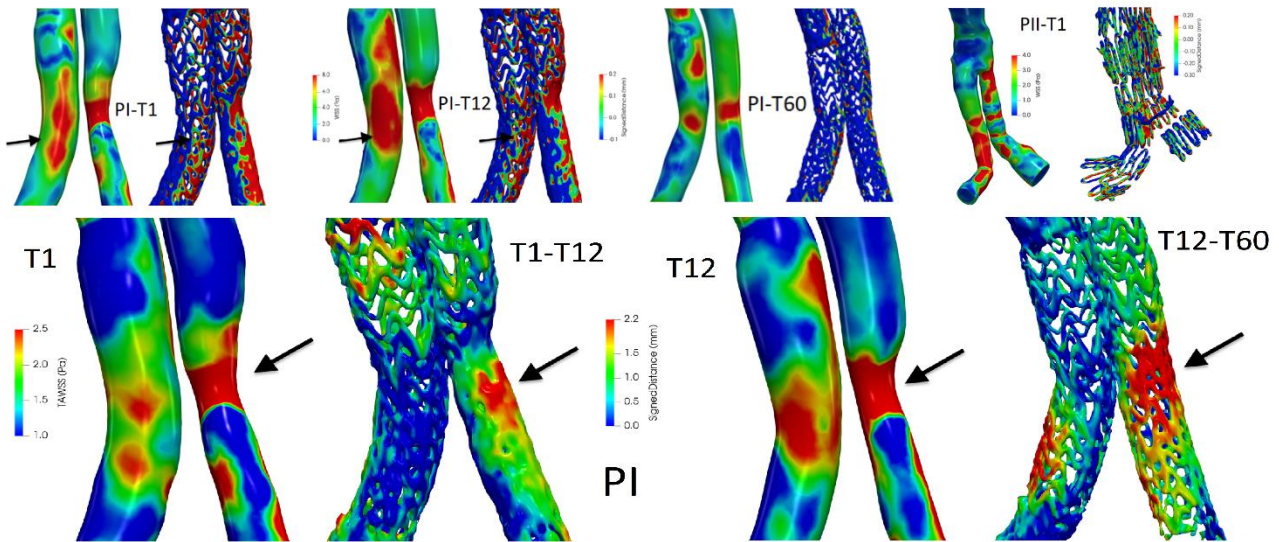


Fig. 4. a) Systolic WSS (left) and IHD (right) for PI-T1, PI-T12, PI-T48, and PII-T1. Arrows highlight the regions of rigid translation in correspondence of elevated WSS localized at the region of iliac branches overlapping in postero-anterior view for both the cases; b) Left: T1-T12 analysis for PI. Right: T12-T60 analysis for PI. For each case, TAWSS is reported on the left and FUD on the right. Arrows highlight regions of large FD in correspondence of elevated TAWSS in postero-anterior view.

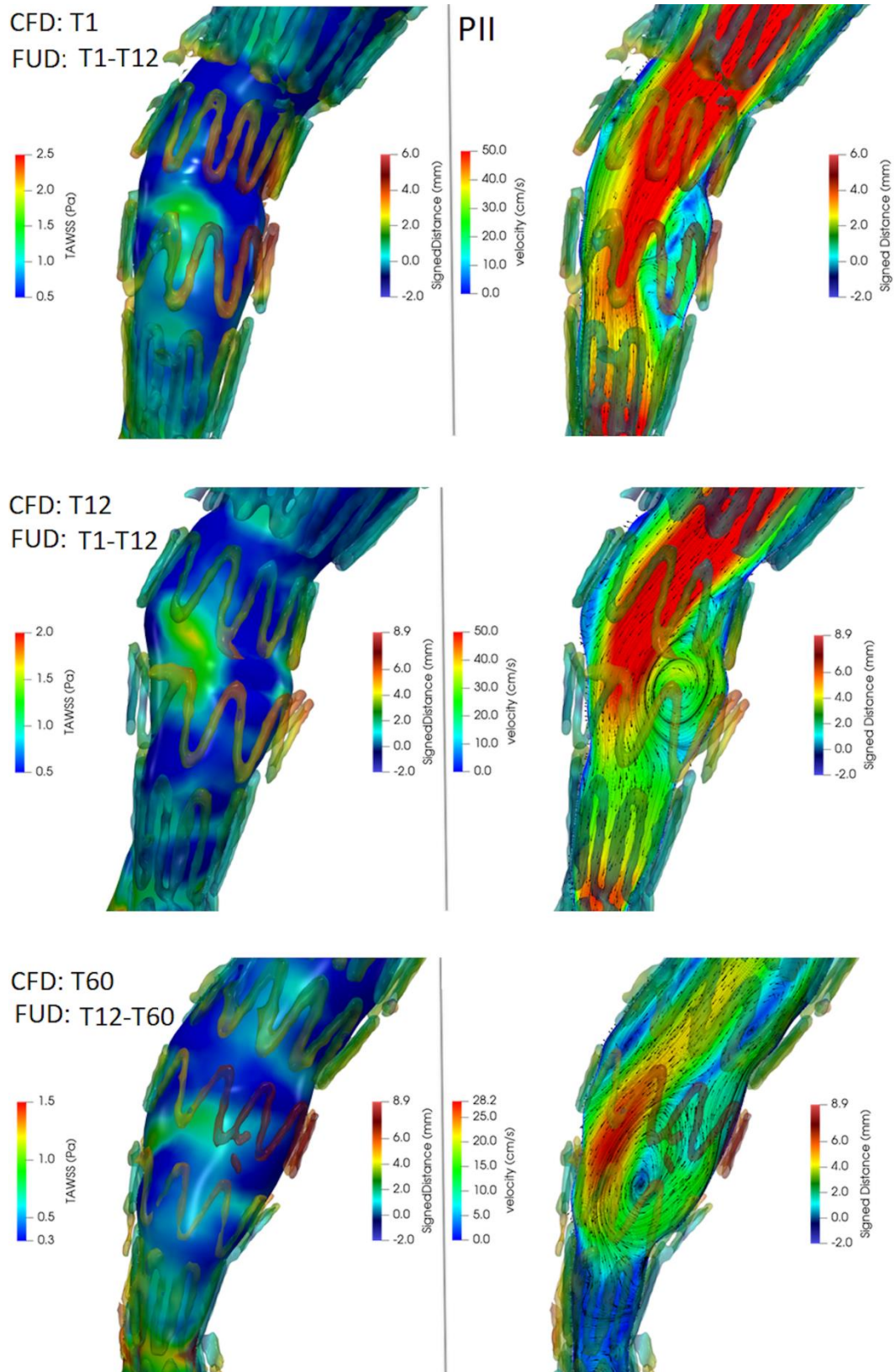


Fig. 5. PII. TAWSS (left) and systolic flow field (right) plots together with FUD. Blood, which initially flows in caudal and slightly anterior direction, impinges the lumen wall at the aortic bending point. The reduction in velocity causes the flow to become unstable, leading to flow separation and recirculation. The expansion of the stent-graft wires results located exactly where such flow disturbances takes place. Coherently with the disturbed flow computation, TAWSS exhibits lower values in the enlarged region with respect to adjacent areas

Tab. 1. Clinical data

	PI	PII
Age (ys)	63	72
Gender	Male	Male
Weight (Kg)	87	87
Height (cm)	1.93	1.70
Body mass index (Kg/m <sup>2</sup> )	23.36	30.10
Blood Pressure (mmHg)	160/80	160/90
Heart rate (bpm)	74	56
AAA diameter (cm)	4.5	4.7
Intrasac Thrombus	No	Yes
Endograft	Excluder GORE	Zenith COOK
Endograft Codes		
Main body	23-12-18	32-82
Right	12-10-00	20-37
Left	14-14-00	22-54

Tab. 2. Maximum endograft FUD displacement over different interval of time in three regions i.e at the level of the aortic main body and at the iliac regions.

	Aortic main body (mm)	Right iliac branch (mm)	Left iliac branch (mm)
PI T1-T12	2.4	2.9	3.6
PI T12-T60	2.6	3.6	3.5
PI T1-T60	5.7	6.4	6.9
PII T1-T12	6.5	4.0	4.4
PII T12-T60	5.6	3.1	3.4
PII T1-T60	8.1	6.2	6.7

## MOX Technical Reports, last issues

Dipartimento di Matematica  
Politecnico di Milano, Via Bonardi 9 - 20133 Milano (Italy)

- 05/2020** Artoli, E.; Beiraoda Veiga, L.; Verani, M.  
*An adaptive curved virtual element method for the statistical homogenization of random fibre-reinforced composites*
- 04/2020** Didkovskyi, O.; Azzone, G.; Menafoglio A.; Secchi P.  
*Social and material vulnerability in the face of seismic hazard: an analysis of the Italian case*
- 02/2020** Fresca, S.; Dede', L.; Manzoni, A.  
*A comprehensive deep learning-based approach to reduced order modeling of nonlinear time-dependent parametrized PDEs*
- 03/2020** Ferro, N.; Micheletti, S.; Perotto, S.  
*Compliance-stress constrained mass minimization for topology optimization on anisotropic meshes*
- 01/2020** Pozzi, S.; Vergara, C.  
*Mathematical and numerical models of atherosclerotic plaque progression in carotid arteries*
- 58/2019** Antonietti, P.F; Manzini, G.; Mourad, H.M.; Verani, M.  
*The virtual element method for linear elastodynamics models. Design, analysis, and implementation*
- 60/2019** Ieva, F; Paganoni, A.M.; Romo, J.; Tarabelloni, N.  
*roahd Package: Robust Analysis of High Dimensional Data*
- 57/2019** Antonietti, P.F.; Bertoluzza, S.; Prada, D.; Verani M.  
*The Virtual Element Method for a Minimal Surface Problem*
- 56/2019** Antonietti, P.F.; Berrone, S.; Borio A.; D'Auria A.; Verani, M.; Weisser, S.  
*Anisotropic a posteriori error estimate for the Virtual Element Method*
- 54/2019** Simona, A.; Bonaventura, L; de Falco, C.; Schoeps, S.  
*IsoGeometric Approximations for Electromagnetic Problems in Axisymmetric Domains*